Hindawi
Advances in Civil Engineering
Volume 2018, Article ID 5267610, 11 pages
https://doi.org/10.1155/2018/5267610

Research Article

Testing of Weakly Weathered Granites of Different Porosities Using a Split Hopkinson Pressure Bar Technique

Lei Yan,[1] Liansheng Liu,[1,2] Shenghui Zhang,[1] Depei Lan,[1] and Jiangchao Liu[3]

[1]*School of Resources and Environmental Engineering, Jiangxi University of Science and Technology, Ganzhou, Jiangxi 341000, China*
[2]*Jiangxi Key Laboratory of Mining Engineering, Ganzhou, Jiangxi 341000, China*
[3]*College of Architecture and Civil Engineering, Beijing University of Technology, Beijing 100022, China*

Correspondence should be addressed to Liansheng Liu; liulsjxust@163.com

Received 11 May 2018; Accepted 6 August 2018; Published 2 September 2018

Academic Editor: Fengqiang Gong

Nuclear magnetic resonance (NMR) and damage impact testing, using a split Hopkinson pressure bar (SHPB) technique, were conducted on weakly weathered granites of different porosities. Based on this, this study determined and analysed the pore structure and distribution, propagation characteristics of stress waves, changes in initial tangent modulus, and energy dissipation in weakly weathered granites of different porosities. The research demonstrated that the nature of the internal porosity of weakly weathered granites changed with total porosity. Pore structure significantly influenced the amplitude of reflected waves and distortion of transmitted waves. Under constant-damage impact loads, the initial tangent modulus decreased with increasing porosity, whereas the stress-strain curves, after reaching the peak stress, had similar shapes. Peak stress and average strain rate showed a strong power-law correlation with porosity, and peak stress decreased in a power-law correlation with the increase of average strain rate. In other words, the difference in average strain resulted from different porosities when the incident energy was same, and the average strain was negatively correlated with porosity. Under damaging impact, the energy absorbed per unit volume decreased with increasing porosity. The research results reveal dynamic characteristics of natural porous rocks under damage impacts, which provide a reference for studying damage effects of porous rocks under the effects of stress waves.

1. Introduction

South Jiangxi Province is the birthplace of ion adsorption-type rare-earth deposits in China, interspersed with a large number and scale of deposits covering a complete range of medium, heavy, and light rare earths, so it is known as "the kingdom of rare earths" [1, 2]. In situ leaching is used in mining therein and the method is highly respected due to the significant environmental protection and cost advantages it affords, while the permeability of the ore body is the key factor restricting its development [3]. For rare-earth ore with a low permeability, the leaching is a slow process and the leaching solution remains in the ore body for a long time, weakening the structure thereof. This causes landslides [4], especially destructive ground floor landslide accidents [5], which hinder the promotion of *in situ* leaching mining technology and exploitation of rare-earth ores. Therefore, in reference to the permeability-increasing methods used in low-permeability oil and gas fields, coal bed methane extraction and gas control and *in situ* leaching of uranium deposits, the assumption of finely controlled blasting of small-dose air-decked charge in a rare-earth ore body has been proposed [6–8]. In the method, the damaging effects of explosive stress waves on rare-earth ore body are used to change internal pore structures, which can improve the permeability of an ore body without inducing its instability and collapse.

Ion adsorption-type rare-earth deposits are generally found to be weathered granites exposed on the ground [2] and explosive packages are generally put in the middle-lower part of semiweathered layers or the upper part of bed rocks. Therefore, by selecting weakly weathered granites in the

lower part of semiweathered layers of rare-earth ore body as research objects, this study investigated the propagation of explosive stress waves in weathered layers of ion adsorption–type rare-earth ore body and the damaging effects of the stress waves on pore structure. In addition, this research studied the dynamic characteristics of weakly weathered granites with different porosities in a rare-earth deposit in Anyuan County [1], Jiangxi Province, China.

Owing to the dynamic characteristics of natural rocks being determined by multiple factors, most scholars studied the dynamic characteristics of porous brittle rock materials by using the split Hopkinson pressure bar (SHPB) test system. Li et al. [9] conducted uniaxial impact and cyclic impact tests on Bukit Timah granites with a similar density by employing a large-diameter SHPB test system. By using these factors, including stress-strain curve, energy dissipation, failure mode, Young's modulus, peak stress, and strain rate, the dynamic characteristics of such granites were characterised. It is found that Young's modulus changes slightly under cyclic impacts and the dynamic fracture strength of the granites is proportional to the cube root of the strain rate. The dynamic mechanical performances of the granites show obvious strain rate, strain-rate hardening, and damage softening effects. The stress-strain curve, before reaching the peak stress, is steep, while the post-peak curve characteristics are correlated with loading rate [10–12]. Zhang and Zhao [13] summarised the dynamic experimental techniques used to assess the mechanical characteristics of brittle rock materials and discussed the factors influencing their initial tangent modulus. Moreover, they proposed that the initial damage suffered by such rocks probably influences the initial tangent modulus, which needs further experimental verification. By analysing the dynamic characteristics of sandstone, Xia et al. [14] constructed artificial rocks, each having different porosities, and studied the influences of porosity on energy dissipation. Ju et al. [15, 16] established a physical model for porous media and used a 3-D finite element model of rocks with different porosities and analysed the stress wave propagation characteristics, the failure mode of specimens, and energy dissipation mechanisms in such porous media, and there is a certain distance from the natural pore rock. By using FLAC^{3D} software to construct 3-D porous models, Ju et al. [17] carried out a numerical simulation of a Brazil disk splitting test on models with different porosities and researched the influences of structural parameters of the pores on the dynamic characteristics of rocks, which provides theoretical support for the development of experimental research.

By employing the nuclear magnetic resonance (NMR) technique [18] and ultrasonic testing technology [19], selected specimens were studied on a layer-by-layer basis, so as to ensure that other conditions remained unchanged except for those pertaining to sample porosity. The damage impact test was conducted on rock specimens with different porosities by using an SHPB test system with a diameter of 50 mm at similar impact velocities. This study recorded the complete impact process and analysed the propagation characteristics of stress waves in natural rocks with different porosities, thus obtaining the stress-strain curves of weakly weathered granites. Furthermore, this research discussed the relationship between initial damage to the rock samples and their initial tangent modulus and analysed the influences of rock porosity on energy dissipation under damaging impacts.

2. Experimental Work

2.1. Preparation of Rock Specimens. The weakly weathered granites used in the test were selected from weakly weathered layers of a rare-earth deposit in Anyuan County, Jiangxi Province, China, and were classified as coarse-grain biotite granites. Such granites were formed in the early Yanshanian and are composed of feldspar, quartz, and biotite, accompanied by small amounts of clay minerals. According to test specifications of rocks for engineering applications, the rough blanks of rock specimens were drilled, cut, and ground into two types of cylindrical specimens, each with a diameter of 50.00 mm and length-diameter ratios of 1.0 and 2.0, respectively. Moreover, the nonparallelism and nonperpendicularity of the end faces were ensured to be less than 0.02 mm in the dynamic load test and 0.05 mm in the static load test. After preparation, the specimens were screened to eliminate those with obvious surface fractures, cracks, and joints: typical specimens are shown in Figure 1.

2.2. Test Devices and Principle

2.2.1. NMR Test and Sample Screening. An NM-60 NMR analyser (Shanghai Niumag Electronic Technology Co., Ltd., China) and a vacuum saturation device were used for testing, and the main magnetic field, magnet control temperature, and frequency of the equipment are 0.52 T, 32 ± 0.02°C, and 22 MHz, respectively. Moreover, the diameter of the magnetic pole is 60 mm and the stability of magnetic field is less than 300 Hz/hour.

After carrying out vacuum-water saturation of the sample, the Carr–Purcel–Meiboom–Gill (CPMG) pulse sequence was tested, and the attenuation signal of the spin echo string was obtained. The signal was the superposition of the water signals in the different sizes of pores, in which the attenuation time of the transverse magnetization vector was T_2 time, which can be expressed as

$$\frac{1}{T_2} = \frac{1}{T_2^1} + \frac{\rho_2 s}{V} + \frac{D(\gamma G T_E)^2}{12}, \quad (1)$$

where T_2^1 is the relaxation time of fluid (ms), ρ_2 is the transverse surface relaxation strength (μm/ms), s is the pore surface area (cm^2), V is the pore volume (cm^3), $\rho_2 s/V$ is the transverse surface relaxation rate, D is the diffusion coefficient, γ is the gyromagnetic ratio, G is the gradient of the magnetic field, is the gradient of the magnetic field (Gs/cm), T_E is the echo time (ms), and $D(\gamma G T_E)^2/12$ is the diffusion relaxation rate. When only one fluid (water) in the pore T_2^1 is neglected, and when the magnetic field is uniform and applied for a short time T_E, the diffusion relaxation rate can also be neglected, then (1) is simplified as

Figure 1: Part of the typical specimens.

$$\frac{1}{T_2} = \frac{1}{T_2^1} + \frac{\rho_2 s}{V}. \tag{2}$$

It is known by formula (2) that the T_2 distribution of the transverse relaxation time can reflect the pore size information, and the total area S around the curve and the transverse axis represents the porosity n_p of the rock samples, the peaks of the T_2 spectrum and the area of the transverse axis S_n (among them $n = 1, 2, \ldots$) represent the volume of a type of pore, and the percentage of each peak area S_n% represents the pore distribution, which can be expressed as

$$S_n\% = \frac{S_n}{S} \times 100\%. \tag{3}$$

2.2.2. Dynamic Mechanical Test. The uniaxial impact and compression test was conducted by using the SHPB test device in Jiangxi University of Science and Technology (Ganzhou city, China). The bar of the SHPB test device, with a diameter of 50.00 mm, was manufactured from 40 Cr alloy steel. The density was 7,810 kg/m^3 and elastic wave velocity was 5400 m/s. The elastic limit and wave impedance were 800 MPa and 42 TPa/s, respectively. In addition, the lengths of the incident, transmitted and absorption bars were 2.0 m, 1.5 m, and 0.5 m, separately. Half-sine stress waves were applied with a spindle-shaped striker, which was able to eliminate P–C oscillation and realise loading of the specimens at a constant strain rate [20, 21]. The diameter and length of the striker were 50.00 mm and 360.10 mm, respectively, and the material used was the same as the bars. The SHPB test device is shown in Figure 2.

By using the SHPB device, a uniaxial impact compression test was conducted on weakly weathered granite specimens with different porosities and a length-diameter ratio of 1.0: each test applied the same incident energy [22, 23]. The incident pulse signal $\varepsilon_I(t)$ and the reflected pulse signal $\varepsilon_R(t)$ in the incident bar and the transmitted pulse signal $\varepsilon_T(t)$ in the transmitted bar were recorded by using data-logged strain gauges. According to one-dimensional stress wave theory, strain rate $\dot{\varepsilon}(t)$, strain $\varepsilon(t)$, and stress $\sigma(t)$ were calculated. Under uniaxial impact compression, the dynamic mechanical parameters deduced from the pulse response of deformation of elastic bars are given by

$$\sigma_d(t) = \frac{A_e}{A} E_e \varepsilon_T(t), \tag{4}$$

$$\begin{aligned} \varepsilon_d(t) &= -\frac{2c_e}{L} \int_0^\tau \varepsilon_R(t)\mathrm{d}t, \\ \dot{\varepsilon}_d(t) &= -\frac{2c_e}{L} \varepsilon_R(t), \end{aligned} \tag{5}$$

where $\dot{\varepsilon}_d(t)$, $\varepsilon_d(t)$, and $\sigma_d(t)$ represent the dynamic compressive stress, the strain, and the strain rate as they changed, over time, under impact loading, respectively. A and L indicate the cross-sectional area and length of the specimens, separately. E_e and A_e denote the sum of the elastic modulus and cross-sectional area of the pressure bar, respectively. c_e denotes the longitudinal wave velocity propagating in the pressure bar and $c_e = \sqrt{E_e/\rho_e}$, where ρ_e represents the density of the pressure bar. The dissipative energy $W_s(t)$ of the specimens was calculated according to the following formula [24]:

$$W_s(t) = W_I(t) - [W_R(t) + W_T(t)], \tag{6}$$

where $W_I(t)$, $W_R(t)$, and $W_T(t)$ indicate the incident energy, the reflected energy, and the transmitted energy, respectively, as given by

$$\begin{aligned} W_I(t) &= E_e c_e A_e \int_0^\tau \varepsilon_I^2(t)\mathrm{d}t, \\ W_R(t) &= E_e c_e A_e \int_0^\tau \varepsilon_R^2(t)\mathrm{d}t, \\ W_T(t) &= E_e c_e A_e \int_0^\tau \varepsilon_T^2(t)\mathrm{d}t. \end{aligned} \tag{7}$$

To compare with the dynamic test, a static uniaxial compression test was conducted on the standard specimens with a length-diameter ratio of 2.0 by using the RMT-150C test system in the Key Laboratory of Mining Engineering (Jiangxi Province, China).

2.3. Testing Procedure. The test process was as follows:

(1) The processed samples were divided into two groups according to the length-diameter ratio. The ratio of length-diameter was 2 for the quasistatic test group and the dynamic test group with the ratio of length-diameter of 1, and the magnetic resonance relaxation measurement for all samples after vacuum saturated water treatment was done.

(2) The test only considered a single factor (the property): to avoid the influence of water [25] and other factors, after the NMR test, all specimens were oven-dried for 24 h at 108°C. After that, the specimens were cooled to room temperature in a desiccator and then removed to measure their mass, dimensions, and ultrasonic wave velocity v_p, so as to eliminate rock specimens with a large discreteness and varying degrees of weathering degrees.

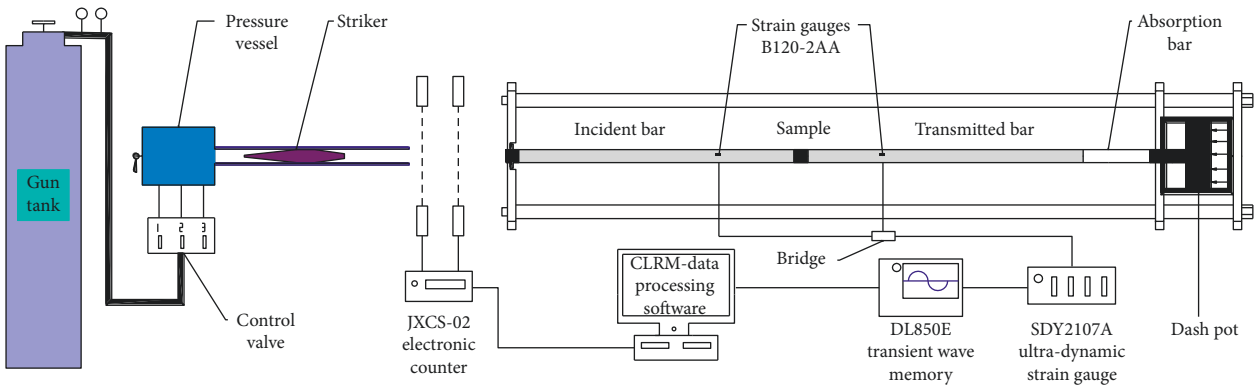

Figure 2: The SHPB test device.

(3) Uniaxial compression tests were carried out on a RMT-150C testing machine in the static test group, and samples with complete stress-strain curves were selected according to the test results.

(4) Combined with NMR test and P-wave velocity test results, the dynamic test group was numbered according to porosity from small to large. On the SHPB test facility, uniaxial impact compression test was carried out by fixing the punch position and nitrogen pressure to control the punch speed at approximately 4 m/s each time. Before the damage impact test, the dynamic force balance of rock samples was tested to ensure the accuracy of the test [26].

3. Results and Discussion

3.1. Pore Structure of Weakly Weathered Granites. The NMR T_2 spectrum reflects the volume distributions of pores with different sizes in rock specimens [18]. A relaxation test was conducted on all specimens and the porosity was calculated. The porosity of 96% of all specimens tested was between 2% and 8%, among which samples with porosity of approximately 2%, 3%, 4%, 5%, 6%, and 7% were selected. Figure 3 shows the distribution curve of T_2 spectra of specimens with different porosities, whereas Figure 4 shows the relationships of area S_n of each peak and its percentage S_n% as well as longitudinal wave velocity v_p with porosity n_p.

As shown in Figure 3, T_2 spectrum curves of weakly weathered granites with different porosities exhibited a similar trend and included two spectral peaks. The first spectral peak S_1 represented small pores, appearing in the vicinity of 0.77 ms, whereas the second, at around 20.52 ms, indicated the presence of large pores. The spectral peaks were connected, which indicated that the dimensions of pores changed continuously. Different specimens did not have identical peak relaxation times, initial relaxation times, and end of relaxation times, and the increments of T_2 spectrum curves with increasing n_p varied. In comparison with fresh granites [18], the mineral particles contained in weakly weathered granites varied more widely in terms of their particle size under the effects of weathering, increasing the differences in the pore distribution in individual specimens.

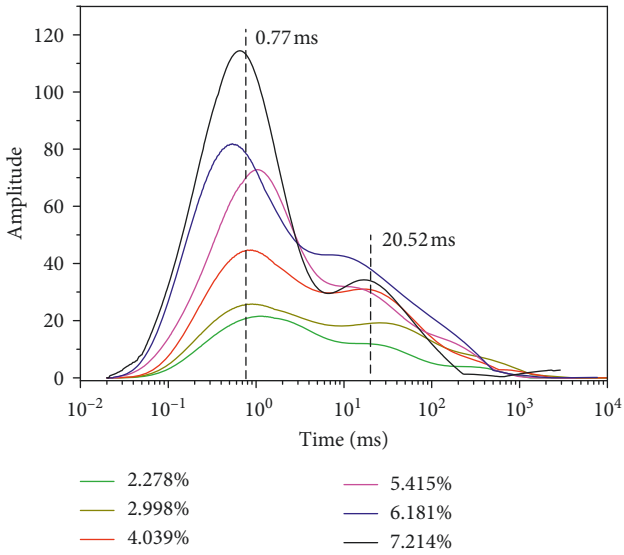

Figure 3: T_2 spectral distribution curve.

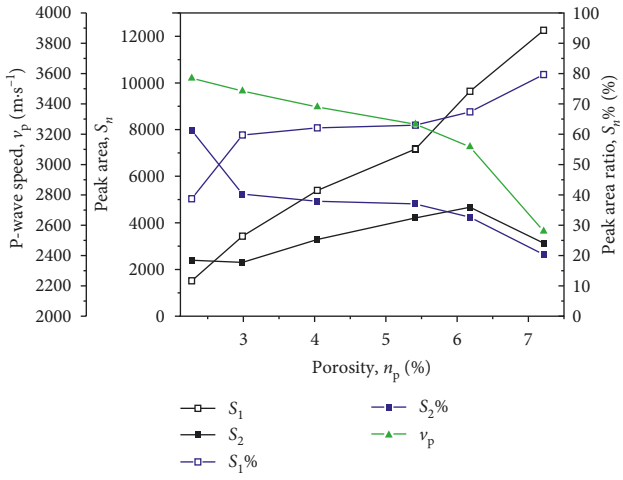

Figure 4: Relationship between n_p and S_n, v_p, and S_n%.

It can be seen from Figure 4 that the numbers of large and small pores both increased with porosity, and large and small pores were distributed uniformly when the porosity changed

between 3% and 6%. Moreover, the ratio of large to small pores was 0.59. Through measurement of the ultrasonic longitudinal wave velocity, v_p, a linearly descending relationship with n_p, which was consistent with the results obtained elsewhere [19], was found: the slope of the line of best fit was negatively correlated with the ratio of large to small pores. The calculation of rock quality index IQ% can be expressed as

$$\mathrm{IQ\%} = \frac{v_p}{v_p'} \times 100\%. \tag{8}$$

Among them, v_p' is the longitudinal wave velocity of rock without fissure and pore condition. The (8) formula was used to calculate the IQ% value, the porosity of the unfractured rock n_p', and the classification of the fracture degree of the rock [27], which can determine the crack degree between the medium and the severity of the crack, and to ensure the consistency of the fracture degree of the specimen.

3.2. Stress Wave Propagation Characteristics. By using the SHPB device, the damage impact dynamic test was carried out on weakly weathered granites. Figure 5 shows the strain signal waveforms of weakly weathered granites with porosities varying from 2.184% to 6.613%, when measured under uniaxial impact compression at impact velocities of between 4.01 and 4.25 m/s.

As seen in Figure 5, the incident, reflected, and transmitted waves were half-sine waveforms. Among them, the amplitude of the incident waves was sensitive to the impact velocity of the striker and increased therewith, whereas the amplitude of the reflected waves depended on the velocity of the striker and the resistance of specimen waves (ρcA). Furthermore, the porosity of the specimens was negatively correlated with density ρ (as shown in Figure 6) and longitudinal wave velocity c (see Section 3.3 for more details). When the difference in the velocity of the striker was insignificant, the reflection coefficient of the specimens increased with increasing porosity [28]. The essence of this behaviour was such that, the reflection times of stress waves increased with the number of pores, so the generated superposition effects of waves [29, 30] uniformly increased the amplitude of the reflected waves. The amplitude of transmitted waves decreased in a step-wise manner with increasing reflection coefficient, which was because different degrees of microelastic deformation and plastic deformation occurred around the pores in the specimens under the effects of propagating stress waves. When the stress waves left the specimens and propagated through the transmitting bar, the elastic strain energy accumulated in the specimens was released in the form of pulses, which acted on the bar, resulting in step-wise attenuation of transmitted waves.

Weakly weathered granites are porous brittle materials, whose fracture toughness K_c is used to describe their ability to resist fracturing. The literature [31–33] shows that fracture toughness is directly proportional to the cube root of the nominal pore dimension, that is, large pores have stronger fracture resistance than small pores. The effects of stress waves on the specimens are shown as follows: large pores undergo microelastic deformation due to compression, irrecoverable plastic deformation occurs in the small pores, and new pores are generated and cracks are connected in solid media. This explained the waveforms of transmitted waves in the specimens with a porosity of 2.184% in which large pores accounted for 61.2% of all pores. Significant accumulated elastic strain energy was released, which caused obvious step-wise changes in the transmitted waves. The closer the ratio of large to small pores in the specimens was to 0.59, the less obvious the step-wise changes. Essentially, pores became more concentrated with the increase of porosity and irreversible deformation occurred around small pores under the effects of the stress waves. Furthermore, cracks generated from small pores extended to, and connected with, large pores, thus weakening, and even losing, the ability of large pores to accumulate elastic strain energy. As a result, the amplitude of transmitted waves decreased with increasing porosity (on the whole), with localised step-changes therein, and the amplitude rose with the reduction of the ratio of large to small pores and was influenced by intergranular cementation. The result reveals that stress waves propagating in porous media not only have a relationship with the number of pores, but also are closely related to pore structure and distribution.

3.3. Stress-Strain Curve. Figures 7 and 8 show the historical curves of stress, strain, and strain rate, and stress-strain behaviours of weakly weathered granites of different porosities under constant-velocity damaging impact as well as stress-strain curve under quasistatic uniaxial compression.

As shown in Figure 7, when the impact velocity of the specimens of weakly weathered granites with different porosities were approximately equal, with increasing porosity, peak stress decreased while the peak strain increased, indicating that the low-porosity specimens had a higher dynamic compressive strength. The stress-time curve shifted to the right before reaching its peak and the depth of the wave trough changed with changing pore size and, in general, increased with increasing porosity. This suggested that microplastic deformation occurred in the specimens and the deformation degree depended on the number, structure, and distribution of pores in the specimens. The peak on the strain-time curve lagged behind the peak stress and decreased with increasing post-peak stress, which indicated that the specimens remained intact and recovered from their previous elastic deformation. The strain rate-time curves of specimens with different porosities showed similar initial growth, reaching peaks in 39 s to 52 s and the time to peak strain rate was delayed and the amplitude increased with increasing porosity. After 87 s, the strain rates of the specimens with different porosities were negative, indicating resilience in the unloading process, corresponding to the later stage of strain-time curve.

As shown in Figure 8(a), the stress-strain curve of weakly weathered granites appeared to be approximately straight before reaching the first maximum and contained a valley from the first maximum to the stress peak. The depth and length of the valley were controlled by pore parameters

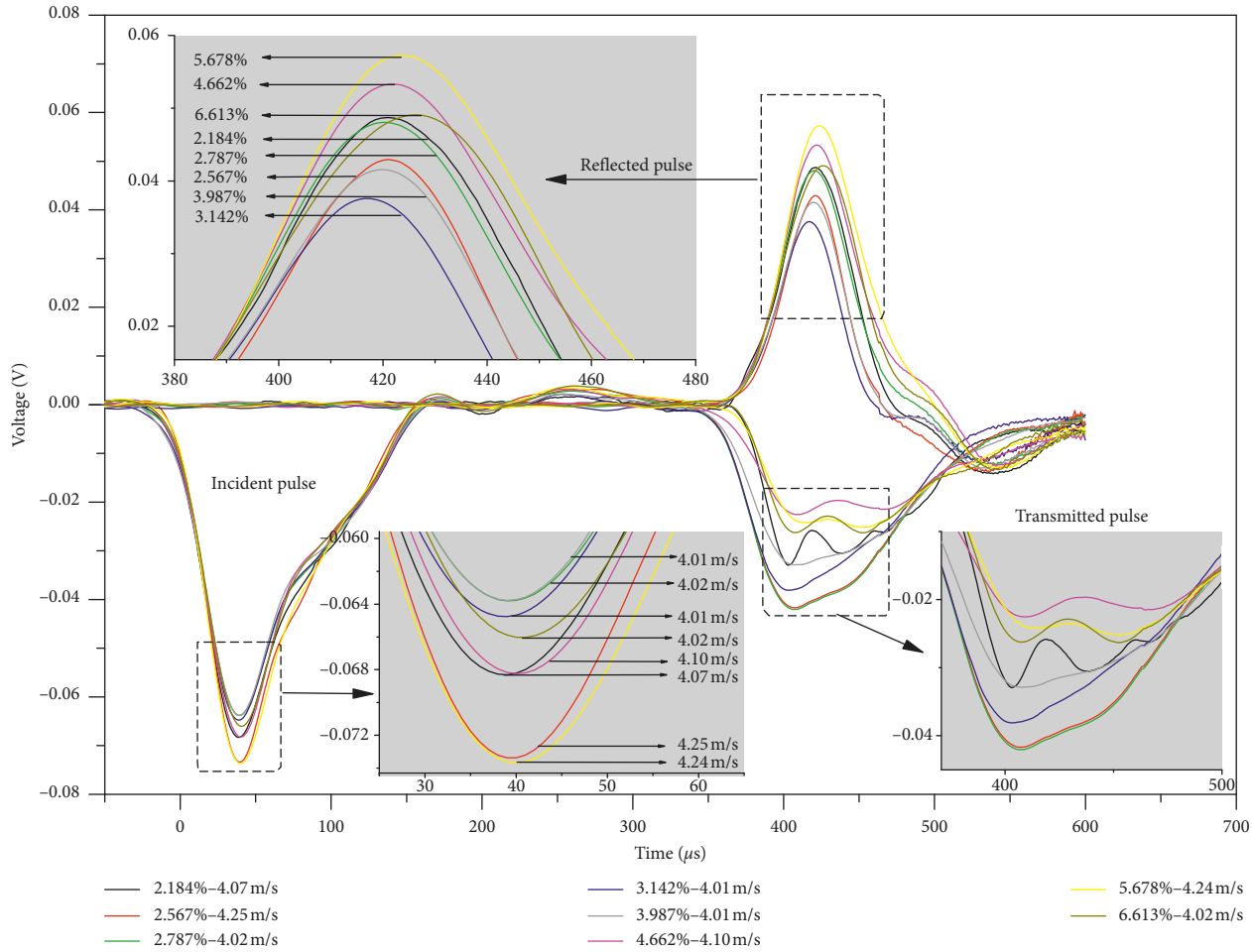

Figure 5: Waveforms of incident, reflected, and transmitted wave strain signals.

(i.e., pore size, shape, and the number of pores) and corresponded to stress- and straintime curves. The specimens remained intact after reaching the peak stress and the stress-strain curve rapidly sprang back and showed a similar shape, which provided evidence counter to that in which the post-peak stress-strain curve was related to impact velocity and extent of damage. The deformation characteristics of specimens in early-stage loading can be characterised by the initial tangent modulus. Under quasistatic loading conditions, with increasing porosity, the compaction stage of pores and fractures in the specimens was more obvious while the initial tangent modulus decreased (Figure 8(b)). When loaded at a moderate strain rate, there was almost no compaction stage but elastic deformation occurred instantly, which matched the test results obtained by Shan et al. [12]. The initial tangent modulus was larger than that in static loading and decreased with increasing porosity; therefore, it can be deduced that the longitudinal wave velocity $c = \sqrt{E/\rho}$ of the specimens was negatively correlated with porosity. The critical strain corresponding to peak stress increased with the porosity. This indicated that the strain rate, critical strain, and peak stress were controlled by the state of pre-existing internal defects when rocks were disturbed by the same dynamic load. When porosity, an important index for

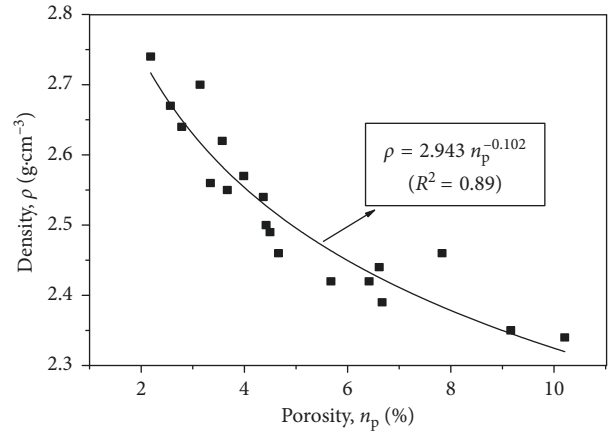

Figure 6: Relationship between porosity and density of weakly weathered granite.

characterising initial defects, changed slightly, stress-strain curves were not completely coincident, demonstrating that pore structure and the pore distribution affected the mechanical properties of rocks. Under static load, the degree of initial defects in rocks was mainly shown by changes in compressive strength and the structure and distribution of

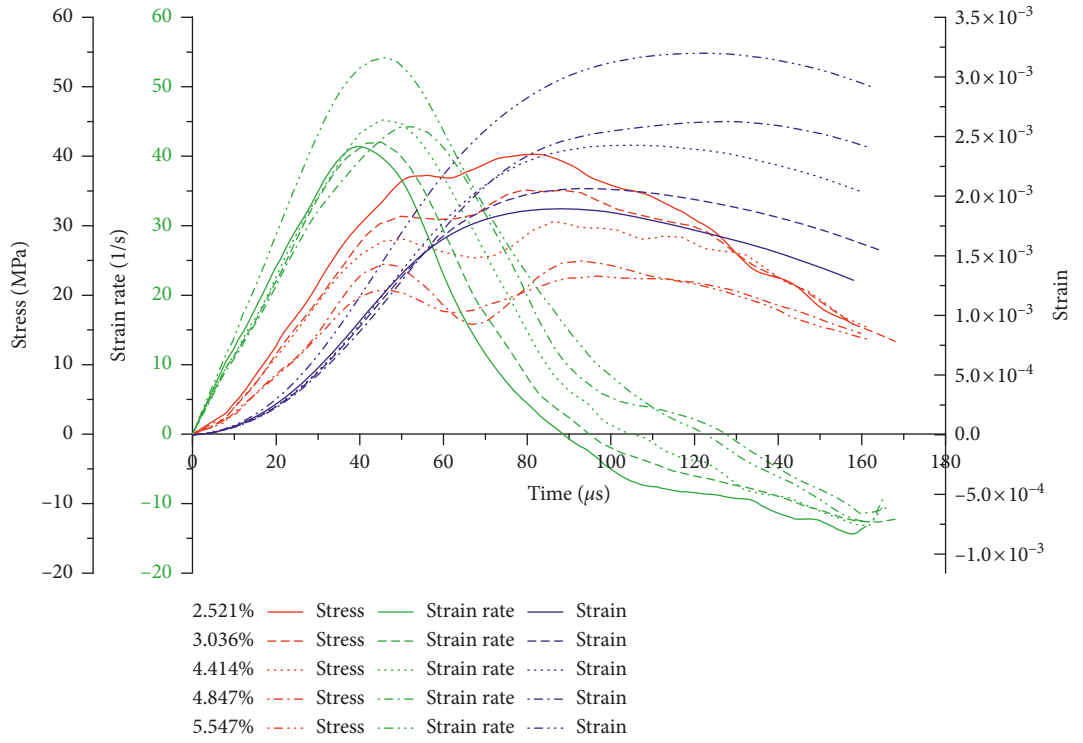

Figure 7: Time history curves of stress, strain, and strain rate of weakly weathered granites with different porosities under uniaxial impact pressure.

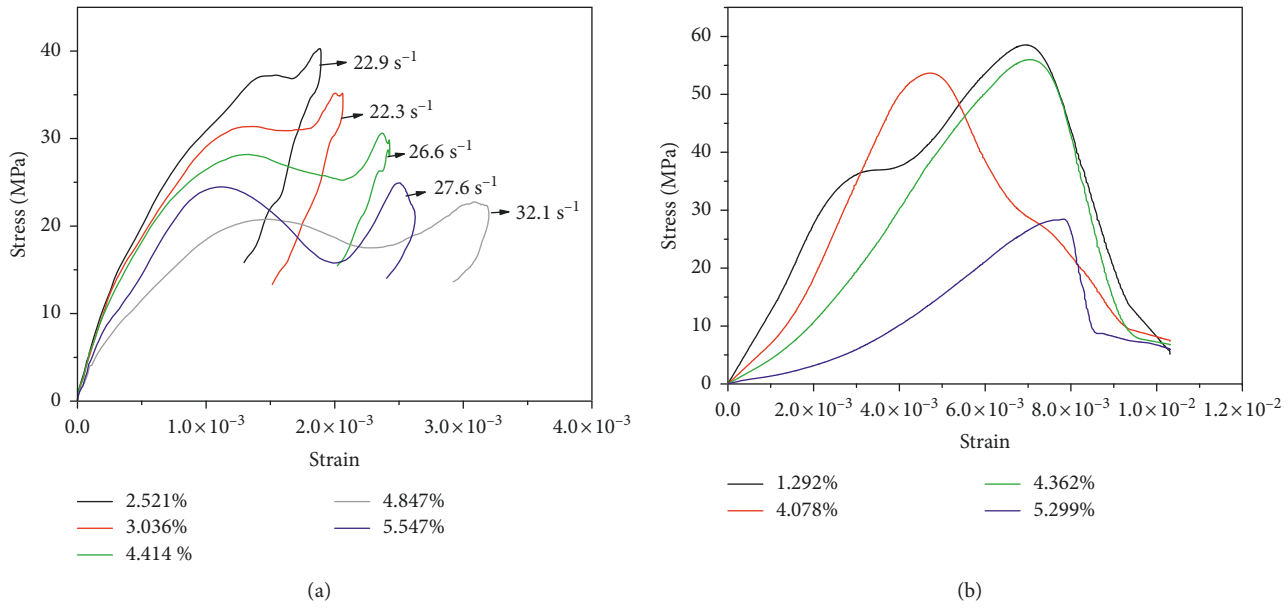

Figure 8: Curve of stress and strain for uniaxial compression of weakly weathered granites with different porosities. (a) High strain rate. (b) Quasistatic.

pores were revealed by the critical strain and the shape of stress-strain curves.

Research into the relationships between initial tangent modulus and critical strain with strain rate remains inconclusive [13]; although it is generally acknowledged that the Young's modulus of rock-like materials increases with increasing strain rate, yet the initial tangent modulus is not influenced by strain rate [9–12, 20, 34–36], whereas the critical strain varies randomly with increasing strain rate [37]. Zhao et al. [38] found that, upon increasing the load rate, Young's modulus decreases slightly and Poisson's ratio increases slightly. By selecting specimens with similar

densities, Li et al. conducted experiments taking the imposed incident energy as the main variable. As illustrated in Figure 6, the density and porosity of an identical batch of specimens exhibit strong correlations, although specimens with the same density show different porosities and specimens having the same porosity present different pore structures and pore distributions. For specimens having the same density and different porosities, the initial tangent modulus decreases with increasing porosity. As for specimens with the same porosity but different pore structures and pore distributions, it is found that the critical strain changes randomly with increasing strain rate. With regard to specimens of the same density and porosity, along with uniformly distributed pores, the initial tangent modulus remains unchanged, being free from the influences of strain rate. The experiments provide evidence for the speculation of Zhang et al. to the effect that initial defects in rocks affect the initial tangent modulus.

Brittle rock materials are relatively sensitive to strain rate under dynamic load [9, 39]. In the SHPB test, strain rate is closely correlated with the velocity of the spindle-shaped striker [40]. Considering this, the stroke of the striker and the pressure delivered by the air pump were adjusted to obtain the same loading rate, so as to explore the influences of porosity on the average strain rate and peak stress and the strain rate effect of porous weakly weathered granites, as shown in Figures 9 and 10.

It can be seen from Figure 9 that the peak stress decreased while the average strain rate increased with increasing porosity, both in a power-law correlation when the weakly weathered granite samples were subjected to impact damage. The average strain rate measures the deformation rate of rock materials under certain loads. The larger the porosity of a rock sample, the more numerous the pores therein: for this kind of rock, the pores bear equal dynamic loads in the short-term under the uniformity hypothesis, so that large and small pores undergo microelastic and microplastic deformation at the same time, and the total deformation depends on the total number of pores and their structural distribution. Therefore, compared with low-porosity specimens, high-porosity specimens show larger total deformation per unit time under the same impact load, which is manifest as a higher strain rate. It can be seen from Figure 10 that the peak stress on the specimen decreased in a power-law correlation with increasing average strain rate, which was contrary to the results of previous research [9, 39, 41]. This inconsistency probably occurs because the strain rate is determined by the impact velocity of the striker, which was taken as the main variable in previous research, while the main variable in the current research is porosity, with the strain rate determined by the presence, and extent of, initial defects in specimens. Formula (3) and Figure 5 explicitly show that the strain rate depends on the amplitude $\varepsilon_R(t)$ of reflected waves and is positively correlated with the porosity. That is to say, the average strain rate is, in essence, a proxy variable for the porosity and explains why the fitting curve of peak stress and average strain rate show a similar trend but differ in value from that fitting the peak stress-porosity data.

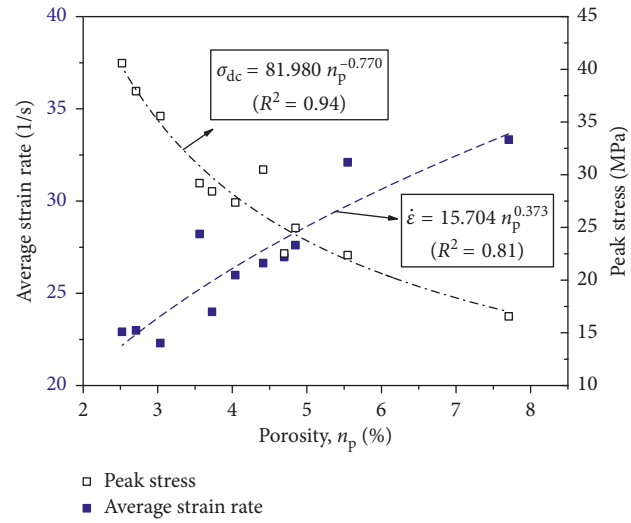

Figure 9: Relationship between porosity, peak stress, and average strain rate.

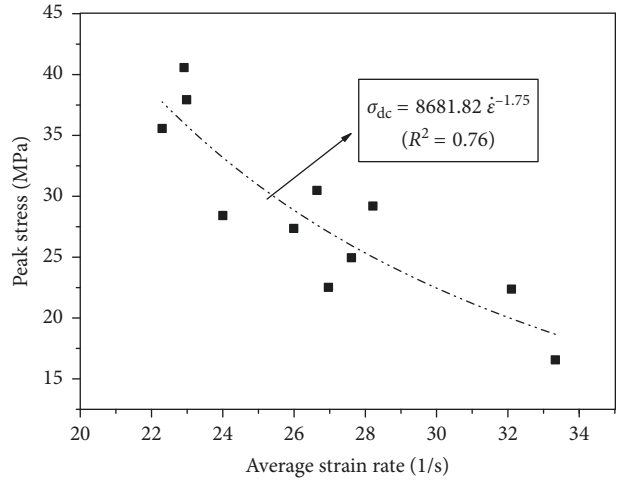

Figure 10: Relationship between average strain rate and peak stress.

3.4. Energy Dissipation. The section analyses the influences of initial defects on the dynamic characteristics of the rocks from an energy perspective. By studying the energy dissipation processes in a sandstone with a porosity of 5.5%, Xia et al. [14] further discussed the energy dissipation in artificial rocks of different porosities (18.5% to 34.5%). Ju et al. [16, 17] established a physical model, and corresponding 3-D finite element model, of rocks with different porosities (5% to 20%) to study the influences of porosity on the energy dissipation of the rocks from two perspectives: physical experiment and numerical simulation. These studies demonstrated that both energy dissipation rate and dissipative energy (absorbed energy) increased with increasing porosity. To avoid errors caused by size discrepancies in the specimens, the energy absorbed per unit volume w_d ($w_d = W_S/V$, where V represents the volume of the specimens [24, 42]) was employed to characterise the relationship between energy dissipation and porosity, as displayed in Figures 11 and 12.

It can be seen from Figure 11 that the curve describing the relationship between energy absorbed per unit volume and porosity declined in a power-law correlation; that is, dissipative energy from the specimens decreased with increasing porosity, which was not consistent with the results obtained in previous research [14, 17]. It was proposed elsewhere [24] that dissipative energy can be divided into energy dissipated due to fracturing, ejection, and other behaviours, among which the ejection-induced dissipative energy accounts for a mere 5% of the total and the dissipative energy caused by other behaviours can be ignored at low loading rates. Therefore, the energy is mainly dissipated due to the extension of original fractures and the initiation of new cracks. In the experiment, specimens generally underwent elastic deformation and microplastic deformation during impact damage: no large fractures were generated and the reflected energy was extremely sensitive to changes in porosity (Figure 12). Meanwhile, the incident energy was approximately constant at a near-constant impact velocity. As the incident energy was near-constant, the reflected energy increased nonlinearly with increasing porosity and its rate of growth was far larger than the rate of reduction of transmitted energy. It can be speculated from formula (4) that the sum of reflected energy and transmitted energy increased with increasing porosity, so the absorbed energy decreased accordingly. Within the tested load range, the compressive stress generated by the incident compression waves met the dynamic fracture criterion of pores with certain sizes, so that these pores were compacted. The waves were reflected on the interfaces of some large pores to produce tensile waves, which formed tensile stress together with the effect of the follow-up incident waves. When the tensile stress satisfied the dynamic fracture criterion of some pores, these pores extended, or new fractures were initiated, while if the tensile stress did not meet the criterion, it was superimposed on the reflected unloading waves such that the reflected energy increased. The results revealed that the rocks exhibited elastic deformation under damaging impact, and irreversible modes of deformation (such as plastic deformation and cracking) did not always increase with the increasing number of pores but were also closely related to the size and distribution thereof.

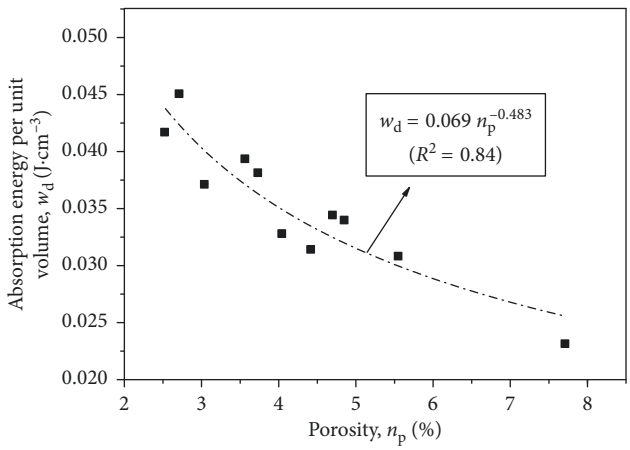

Figure 11: Relationship between porosity and absorption energy per unit volume.

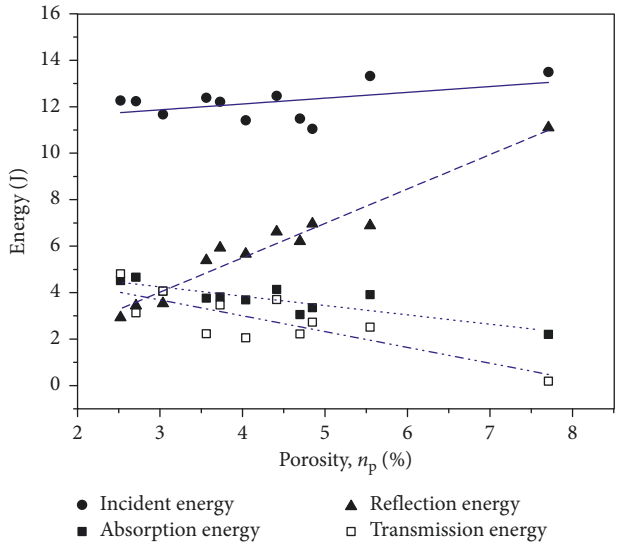

Figure 12: Relationship between porosity and energy.

4. Conclusions

The structural and distribution characteristics of pores in weakly weathered granites with different porosities were ascertained through interpretation of NMR test data. Then, specimens with different porosities and similar pore structures and pore distributions were selected for quasi-static uniaxial compression, and SHPB uniaxial compression and impact, testing. On this basis, we analysed the propagation characteristics of stress waves, the stress-strain curves of porous rock samples, and the energy dissipation mechanism governing the impact process in rocks with different porosities using the SHPB technique. In addition, the changes in initial tangent modulus and critical strain were discussed. The following conclusions were drawn:

(1) The incident waves were sensitive to the impact velocity during the impact damage of these weakly weathered granites, and a minor change in the impact velocity was able to cause corresponding fluctuations in the incident waves which were not influenced by the pores. Due to the superimposed effect of these incident waves, the amplitude of the reflected waves increased significantly with increasing porosity. The distortion of the transmitted waves was controlled by the pore structure and distribution, with their amplitude decreased with increasing porosity.

(2) The times taken for the specimens to reach peak dynamic stress, peak strain, and peak strain rate were all prolonged with increasing porosity and the stress waves propagated more slowly in high-porosity rocks, which indicated that porous media have an attenuating effect on stress wave propagation. The

peak dynamic stress decreased with increasing porosity, which was consistent with the fact that the compressive strength of the specimens decreased with increasing porosity under quasistatic loading.

(3) The initial tangent modulus was determined by the extent of the initial damage to the rock samples. At a constant loading rate, the initial tangent modulus decreased with increasing porosity, and the initial tangent modulus presented the same trend under quasistatic loading.

(4) At a constant impact velocity, the energy absorbed per unit volume in these weakly weathered granite samples with different porosities decreased in a power-law correlation with the increasing porosity. The rocks underwent elastic deformation under impact damage, with the reflected energy linearly increasing while the transmitted and absorbed energies linearly decreased with the increasing porosity. A higher porosity did not always lead to greater energy dissipation which was also associated with the loading rate, pore structure, and pore distribution.

This research was only focused on analysis of the mechanical properties of weakly weathered granites with porosities of between 2% and 8% under impact damage. The mechanical properties of rocks, with other porosities, and under heavier impacts, remain to be studied through experimental and theoretical means.

Data Availability

The (TIFF of figure) data used to support the findings of this study are included within the article.

Conflicts of Interest

The authors declare no conflicts of interest regarding the publication of this paper.

Acknowledgments

The work was supported by a project funded by the National Natural Science Foundation of China (51404111), China Scholarship Council (201708360023), China Postdoctoral Science Foundation (2014M562529XB), Jiangxi Provincial Education Department (GJJ160643), and the Programme of Qingjiang Excellent Young Talents, Jiangxi University of Science and Technology, China. The aforementioned financial supports are much appreciated.

References

[1] L. Zhang, K. X. Wu, L. K. Chen, P. Zhu, and H. Ouyang, "Overview of metallogenic features of ion-adsorption type REE deposits in southern Jiangxi province," *Journal of the Chinese Society of Rare Earths*, vol. 33, no. 1, pp. 10–17, 2015.

[2] R. A. Chi and J. Tian, "A review of weathered crust rare earth ore," *Journal of the Chinese Society of Rare Earths*, vol. 25, no. 6, pp. 641–650, 2007.

[3] Y. X. Li, L. Zhang, and X. M. Zhou, "Resource and environment protected exploitation model for ion-type rare earth deposit in southern of China," *Chinese Rare Earths*, vol. 31, no. 2, pp. 80–85, 2010.

[4] Z. B. Huang, C. Cai, X. Q. Yuan et al., "Simple analysis for safety problems in the in-situ leaching mining of ionic rare earth mine," *Chinese Rare Earths*, vol. 34, no. 4, pp. 99–102, 2013.

[5] X. Z. Tang, M. N. Li, and D. Yang, "Slope slide in in-situ leaching of ionic type rare-earth ore and its countermeasures," *Metal Mine*, vol. 289, no. 7, pp. 6–8, 2000.

[6] Y. S. Ding, L. Chen, X. Xie et al., "On the stimulation with 'exploding in fractures' in low permeability reservoirs," *Petroleum Exploration and Development*, vol. 28, no. 2, pp. 90–96, 2001.

[7] Y. Q. Zhao, D. Yang, Y. Q. Hu et al., "Study on the effective technology way for mining methane in low permeability coal seam," *Journal of China Coal Society*, vol. 6, no. 5, pp. 455–458, 2001.

[8] W. Wang, X. C. Li, W. Yuan et al., "Model test and mechanism study of the blasting-enhanced permeability of sandstone-type uranium deposits of low-permeability," *Chinese Journal of Rock Mechanics and Engineering*, vol. 35, no. 8, pp. 1609–1617, 2016.

[9] X. B. Li, T. S. Lok, and J. Zhao, "Dynamic characteristics of granite subjected to intermediate loading rate," *Rock Mechanics and Rock Engineering*, vol. 38, no. 1, pp. 21–39, 2005.

[10] X. T. Ren, T. Q. Zhou, F. P. Zhong et al., "Experimental study for the dynamic mechanical behavior of granite," *Journal of Experimental Mechanics*, vol. 25, no. 6, pp. 723–730, 2010.

[11] J. F. Liu, S. S. Hu, Y. Y. Hu, and J. Zhao, "Research on dynamic compressive testing and mechanics properties of granite," *Chinese Journal of Rock Mechanics and Engineering*, vol. 19, no. 5, pp. 618–621, 2000.

[12] R. L. Shan, S. L. Chen, and B. Q. Li, "Experimental study of granite constitutive properties under uniaxial impact," *Explosion and Shock Waves*, vol. 20, no. 1, pp. 32–38, 2000.

[13] Q. B. Zhang and J. Zhao, "A Review of dynamic experimental techniques and mechanical behaviour of rock materials," *Rock Mechanics and Rock Engineering*, vol. 47, no. 4, pp. 1411–1478, 2014.

[14] C. J. Xia, H. P. Xie, and Y. Ju, "SHPB test on porous rock," *Chinese Journal of Rock Mechanics and Engineering*, vol. 25, no. 5, p. 896, 2006.

[15] Y. M. Yang, Y. Ju, H. S. Liu, and H. J. Wang, "Influence of porous structure properties on mechanical performances of rock," *Chinese Journal of Rock Mechanics and Engineering*, vol. 28, no. 10, pp. 2031–2038, 2009.

[16] Y. Ju, Y. M. Yang, Y. Z. Mao et al., "Laboratory investigation on mechanisms of stress wave propagations in porous media," *Science in China Series E: Technological Sciences*, vol. 39, no. 5, pp. 904–918, 2009.

[17] Y. Ju, H. J. Wang, Y. M. Yang et al., "Numerical simulation of mechanisms of deformation, failure and energy dissipation in porous rock media subjected to wave stresses," *Science in China Technological Sciences*, vol. 40, no. 6, pp. 711–726, 2010.

[18] K. P. Zhou, J. L. Li, Y. J. Xu, and Y. M. Zhang, "Measurement of rock pore structure based on NMR technology," *Journal of Central South University (Science and Technology)*, vol. 43, no. 12, pp. 4796–4800, 2012.

[19] L. M. del Río, F. López, F. J. Esteban et al., "Ultrasonic characterization of granites obtained from industrial quarries of Extremadura (Spain)," *Ultrasonics*, vol. 44, no. 8, pp. e1057–e1061, 2006.

[20] F. J. Chu, D. W. Liu, M. Tao, and H. D. Peng, "Dynamic response of sandstones with different water contents based on SHPB," *Chinese Journal of Engineering*, vol. 39, no. 12, pp. 1783–1790, 2017.

[21] M. Tao, A. Ma, W. Cao et al., "Dynamic response of pre-stressed rock with a circular cavity subject to transient loading," *International Journal of Rock Mechanics and Mining Sciences*, vol. 99, pp. 1–8, 2017.

[22] F. Dai, S. Huang, K. Xia, and Z. Tan, "Some fundamental issues in dynamic compression and tension tests of rocks using split Hopkinson pressure bar," *Rock Mechanics and Rock Engineering*, vol. 43, no. 6, pp. 657–666, 2010.

[23] F. Q. Gong, B. X. Li, Q. H. Rao et al., "Reference method for determining sample size in SHPB tests of rock materials," *Journal of Vibration and Shock*, vol. 32, no. 17, pp. 24–28, 2013.

[24] Q. Ping, X. Luo, Q. Y. Ma, and P. Yuan, "Broken energy dissipation characteristics of sandstone specimens under impact loads," *Chinese Journal of Rock Mechanics and Engineering*, vol. 32, no. s2, pp. 4197–4203, 2015.

[25] W. Wu and J. Zhao, "Effect of water content on P-wave attenuation across a rock fracture filled with granular materials," *Rock Mechanics and Rock Engineering*, vol. 48, no. 2, pp. 867–871, 2015.

[26] T. B. Yin, L. Bai, X. Liu et al., "Effect of thermal treatment on the mode I fracture toughness of granite under dynamic and static coupling load," *Engineering Fracture Mechanics*, vol. 199, pp. 143–158, 2018.

[27] R. M. Goodman, *Introduction to Rock Mechanics*, John Willey and Sons, New York, NY, USA, 1980.

[28] L. L. Wang, *Foundation of Stress Waves*, National Defense Industry Press, Beijing, China, 2005.

[29] Y. Zou, J. Li, L. He et al., "Wave propagation in the vicinities of rock fractures under obliquely incident wave," *Rock Mechanics and Rock Engineering*, vol. 49, no. 5, pp. 1789–1802, 2016.

[30] J. B. Zhu, X. B. Zhao, W. Wu, and J. Zhao, "Wave propagation across rock joints filled with viscoelastic medium using modified recursive method," *Journal of Applied Geophysics*, vol. 86, no. 11, pp. 82–87, 2012.

[31] S. Z. Yin, *Fracture, Damage Theory and Application*, Tsinghua University Press, Beijing, China, 1992.

[32] T. Y. Fan, *The Principle and Application of Dynamic Facture*, Beijing Institute of Technology Press, Beijing, China, 2006.

[33] F. Q. Gong, D. H. Lu, Q. H. Rao et al., "Toughness increasing or decreasing effect of hard rock fracture with pre-static loading under dynamic disturbance," *Chinese Journal of Rock Mechanics and Engineering*, vol. 33, no. 9, pp. 1905–1915, 2014.

[34] P. H. Bischoff and S. H. Perry, "Compressive behaviour of concrete at high strain rates," *Materials and Structures*, vol. 24, no. 6, pp. 425–450, 1991.

[35] D. J. Frew, M. J. Forrestal, and W. A. Chen, "A split Hopkinson pressure bar technique to determine compressive stress-strain data for rock materials," *Experimental Mechanics*, vol. 41, no. 1, pp. 40–46, 2001.

[36] X. B. Li, F. Q. Gong, M. Tao et al., "Failure mechanism and coupled static-dynamic loading theory in deep hard rock mining: a review," *Journal of Rock Mechanics and Geotechnical Engineering*, vol. 9, no. 4, pp. 767–782, 2017.

[37] R. D. Perkins, S. J. Green, and M. Friedman, "Uniaxial stress behavior of porphyritic tonalite at strain rates to 10^3/second," *International Journal of Rock Mechanics & Mining Sciences & Geomechanics Abstracts*, vol. 7, no. 5, pp. 527–535, 1970.

[38] J. Zhao, H. B. Li, M. B. Wu et al., "Dynamic uniaxial compression tests of a granite," *International Journal of Rock Mechanics and Mining Sciences*, vol. 36, no. 2, pp. 273–277, 1999.

[39] L. Hong, B. X. Li, C. D Ma et al., "Study on size effect of rock dynamic strength and strain rate sensitivity," *Chinese Journal of Rock Mechanics and Engineering*, vol. 27, no. 3, pp. 526–533, 2008.

[40] K. Xia and W. Yao, "Dynamic rock tests using split Hopkinson (Kolsky) bar system-A review," *Journal of Rock Mechanics and Geotechnical Engineering*, vol. 7, no. 1, pp. 27–59, 2015.

[41] B. W, B. X. Li, T. B. Yin et al., "Split Hopkinson pressures bar (SHPB) experiments on dynamic strength of water-saturated sandstone," *Chinese Journal of Rock Mechanics and Engineering*, vol. 29, no. 5, pp. 1003–1009, 2010.

[42] T. B. Yin, K. Peng, L. Wang et al., "Study on impact damage and energy dissipation of coal rock exposed to high temperatures," *Shock and Vibration*, vol. 21, pp. 1–10, 2016.